

Selective Knowledge Sharing for Privacy-Preserving Federated Distillation without A Good Teacher

Jiawei Shao¹, Fangzhao Wu^{2,*}, and Jun Zhang^{1,*}

¹Hong Kong University of Science and Technology, Hong Kong

²Microsoft Research Asia, Beijing

*correspondce: Jun Zhang (eejzhang@ust.hk), Fangzhao Wu (wufangzhao@gmail.com)

ABSTRACT

While federated learning is promising for privacy-preserving collaborative learning without revealing local data, it remains vulnerable to white-box attacks and struggles to adapt to heterogeneous clients. Federated distillation (FD), built upon knowledge distillation—an effective technique for transferring knowledge from a teacher model to student models—emerges as an alternative paradigm, which provides enhanced privacy guarantees and addresses model heterogeneity. Nevertheless, challenges arise due to variations in local data distributions and the absence of a well-trained teacher model, which leads to misleading and ambiguous knowledge sharing that significantly degrades model performance. To address these issues, this paper proposes a *selective knowledge sharing* mechanism for FD, termed *Selective-FD*. It includes client-side selectors and a server-side selector to accurately and precisely identify knowledge from local and ensemble predictions, respectively. Empirical studies, backed by theoretical insights, demonstrate that our approach enhances the generalization capabilities of the FD framework and consistently outperforms baseline methods. This study presents a promising direction for effective knowledge transfer in privacy-preserving collaborative learning.

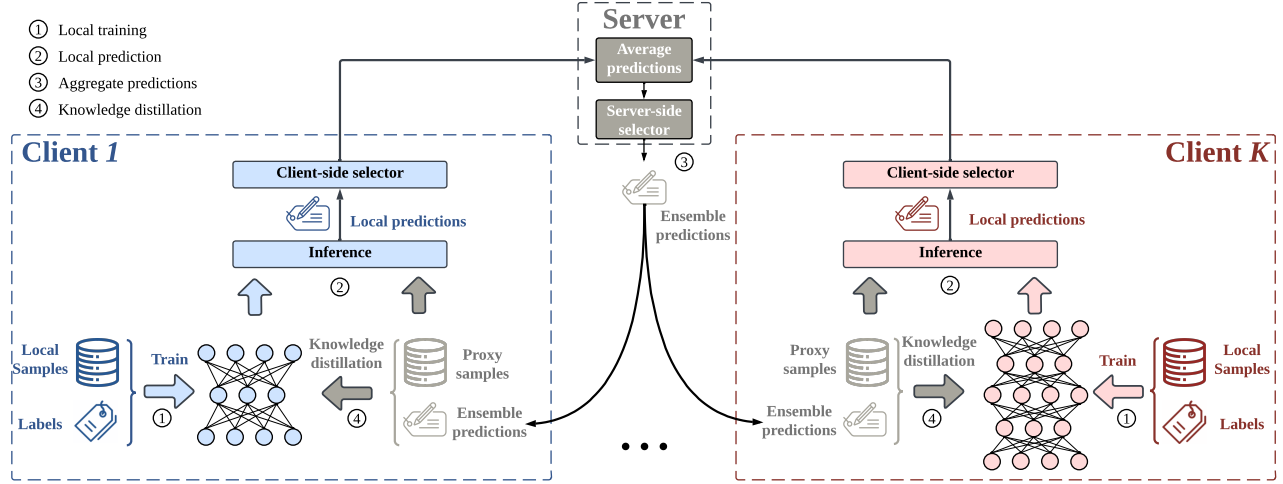


Figure 1. The overall framework of Selective-FD. Each client owns a private local dataset and a personalized model. To transfer knowledge in each communication round, the clients upload the local predictions of proxy samples to the server for aggregation, and the ensemble predictions are sent back to clients for knowledge distillation. The client-side selectors and the server-side selector are responsible for filtering out misleading and ambiguous knowledge from the clients’ predictions.

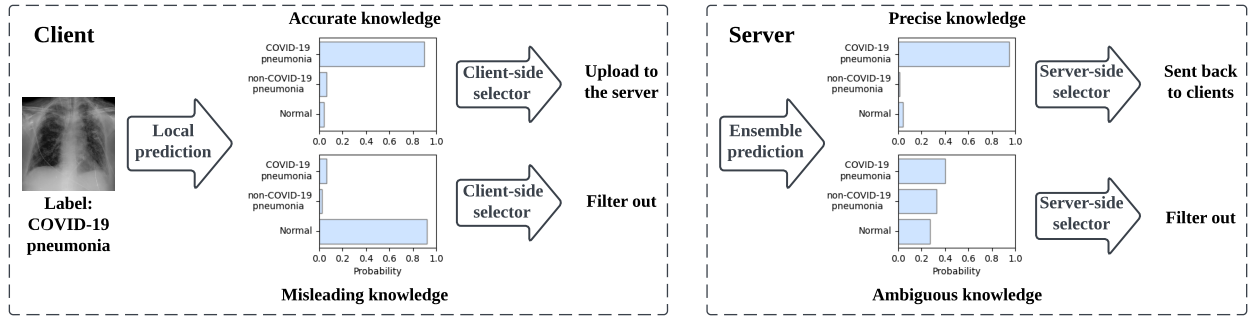


Figure 2. An example of a proxy sample from the pneumonia detection task and its corresponding prediction on a client (left) or the server (right). The output prediction takes the form of a soft label (i.e., a logits vector), where each element represents the probability of the corresponding label. The predicted label is the element with the highest probability. We measure the quality of knowledge in federated distillation by accuracy and precision. The accurate prediction matches the ground truth label, while misleading knowledge does not. Meanwhile, precise knowledge has low entropy, while ambiguity implies high entropy and uncertainty. The client-side selectors are responsible for filtering out incorrect local predictions, while the server-side selector aims to eliminate ambiguous knowledge.

The rapid development of deep learning (DL)¹ has paved the way for its widespread adoption across various application domains, including medical image processing², intelligent healthcare³, and robotics⁴. The key ingredients of DL include massive datasets and powerful computing platforms, which makes centralized training a typical approach for building high-performing models. However, regulations such as the General Data Protection Regulation (GDPR)⁵ and California Consumer Privacy Act (CCPA)⁶ have been implemented to limit data collection and storage since the data may contain sensitive personal information. For instance, collecting chest X-ray images from multiple hospitals to curate a large dataset for pneumonia detection is practically difficult, since it would violate patient privacy laws and regulations such as Health Insurance Portability and Accountability Act (HIPAA)⁷. While these restrictions as well as regulations are essential for privacy protection, they hinder the utilization of centralized training in practice. Meanwhile, many domains face the “data islands” problem. For instance, individual hospitals may possess only a limited number of data samples for rare diseases, which makes it difficult to develop accurate and robust models based on local private data.

Federated learning (FL)^{8,9} is a promising technique that can effectively utilize distributed data while preserving privacy.

In particular, multiple data-owning clients collaboratively train a DL model by updating models locally on private data and aggregating them globally. These two steps iterate many times until convergence, while private data is kept local. Despite many benefits, FL faces challenges and poses new inconveniences. Specifically, the periodical model parameter exchange in FL entails communication overhead that scales up with the model size. This prohibits the use of large-sized models in FL^{10,11}, which severely limits the model accuracy. Besides, standard federated training methods enforce local models to adopt the same architecture, which cannot adapt well to heterogeneous clients equipped with different computation resources^{12,13}. Furthermore, although the raw data are not directly shared among clients, the model parameters may encode private information about datasets. It has recently been demonstrated that transferring knowledge via model aggregation is vulnerable to white-box attacks^{14,15}.

To resolve the above difficulties of FL requires us to rethink the fundamental problem of privacy-preserving collaborative learning, which is to effectively share *knowledge* among distributed clients while preserving privacy. In addition to model aggregation in FL, knowledge distillation (KD)¹⁶ is an effective technique for transferring knowledge from a well-trained teacher model to student models by leveraging an unlabeled proxy dataset. The inference results on the proxy samples represent *privileged* knowledge to supervise the training of the student models. Applying KD to collaborative learning gives rise to a new paradigm called federated distillation (FD)^{17–19}, where the ensemble of clients’ local predictions on the proxy samples serves as privileged knowledge. By sharing the hard labels (i.e., predicted results)²⁰ of proxy samples instead of model parameters, the FD framework largely reduces the communication overhead, is able to support heterogeneous local models, and is free from white-box attacks. Despite the potential for improving efficiency and privacy, FD is sensitive to the training state of local models due to the lack of a well-trained teacher, where the ensemble predictions may have low quality due to the under-fitted local predictors. Besides, the non-identically independently distributed (non-IID) data distributions^{21,22} across clients exacerbate this issue, since the local models cannot output accurate predictions on the proxy samples that are outside their local distributions²³. To address the negative impact of misleading knowledge, an alternative is to incorporate soft labels (i.e., normalized logits)¹⁶ during knowledge distillation to enhance the generalization performance. Soft labels provide rich information about the relative similarity between different classes, enabling student models to generalize effectively to unseen examples. However, a previous study¹⁸ noted that ensemble predictions may be ambiguous and exhibit high entropy when predictions of clients are inconsistent. Sharing soft labels can exacerbate this problem as they are less certain than hard labels. The misleadingness and ambiguity harm the knowledge distillation and local training. For instance, in our experiments on image classification tasks, existing FD methods barely outperform random guessing with severe non-IID distributions.

This work aims to tackle the challenge of knowledge sharing in FD without a good teacher, and our key idea is to filter out misleading and ambiguous knowledge. We proposed a *selective knowledge sharing* mechanism in federated distillation (named *Selective-FD*) to identify accurate and precise knowledge during the federated training process. As shown in Fig. 1 and Fig. 2, this mechanism comprises client-side selectors and a server-side selector. At each client, we constructed a selector to identify out-of-distribution (OOD) samples^{24,25} from the proxy dataset based on the density-ratio estimation²⁶, which detects outliers by quantifying the difference in densities between the inlier distribution and outlier distribution. If the density ratio of a particular sample is close to zero, the client considers it an outlier and refrains from sharing the predicted result to prevent misleading other clients. On the server side, we average the uploaded predictions from the clients and filter out the ensemble predictions exhibiting high entropy and representing ambiguous knowledge. The selected ensemble predictions are then returned to the clients for knowledge distillation. We provided theoretical insights to demonstrate the impact of our selective knowledge sharing mechanism on the training convergence, and we evaluate Selective-FD in two applications, including a pneumonia detection task and three benchmark image classification tasks. Extensive experimental results show that Selective-FD excels in handling non-IID data and significantly improves test accuracy compared to the baselines. Remarkably, Selective-FD with hard labels achieves performances close to the one sharing soft labels. Furthermore, our proposed Selective-FD reduces the communication cost of the standard FedAvg approach by up to 900×. We believe that the proposed method will serve as a valuable tool for training large models in the federated framework for future applications.

Results

Performance Evaluation

The experiments are conducted on a pneumonia detection task²⁷ and three benchmark image classification tasks^{28–30}. The pneumonia detection task aims to detect pneumonia from chest X-ray images. This task is based on the COVIDx dataset²⁷ that contains three classes as shown in Fig. 3(a), including normal people, non-COVID-19 infection, and COVID-19 viral infection. We consider four clients, e.g., hospitals, in the federated distillation framework. To simulate the non-IID data across clients, each of them only has one or two classes of chest X-ray images with 1,000 images for each class. Besides, we construct a proxy dataset for knowledge transfer, which contains all three classes and each class has 500 unlabeled samples. A visualization of the statistical heterogeneity of the datasets is shown in Fig. 3(b). The test dataset consists of 100 normal images and 100 images of pneumonia infection, where half of the pneumonia infections are non-COVID-19 infections and the other half are COVID-19

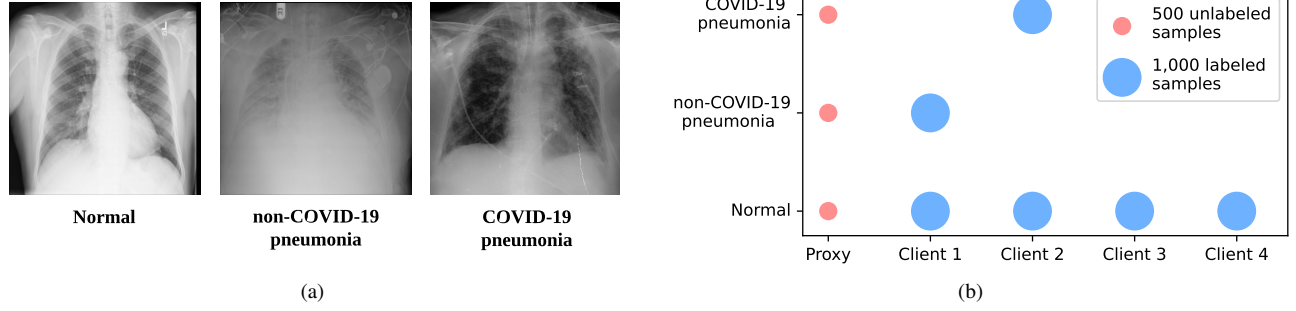


Figure 3. Overview of federated distillation on the pneumonia detection task. (a) Example chest X-ray images of normal people, non-COVID-19 infection, and COVID-19 viral infection. (b) Visualization of non-IID data distribution. The horizontal axis indexes the proxy dataset and the local datasets, while the vertical axis indicates class labels. The size of scattered points denotes the number of samples.

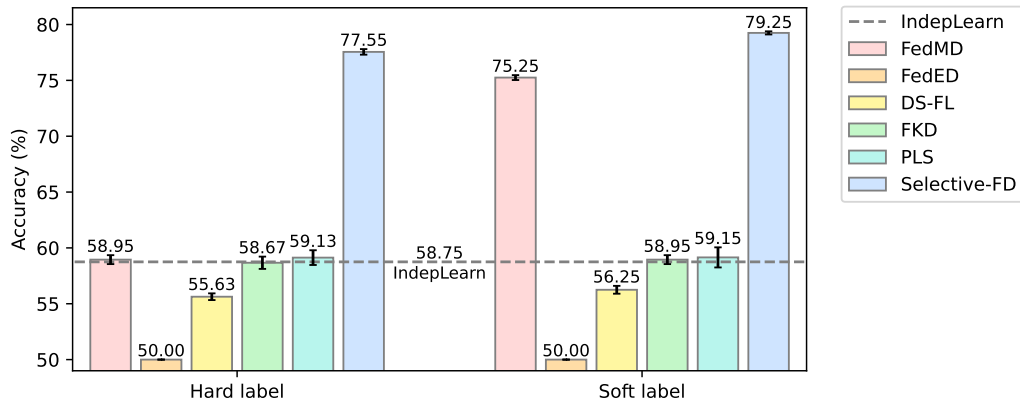


Figure 4. Test accuracy of different methods on the pneumonia detection task. The error bar represented the standard deviations calculated from five repetitions. The results show that the proposed Selective-FD method achieves the best performance, and the accuracy gain is more significant when using hard labels to transfer knowledge. Specifically, some baselines perform even worse than the independent learning scheme. These results demonstrate that knowledge sharing among clients can mislead and negatively influence local training.

infections. Moreover, we evaluate the proposed method on three benchmark image datasets, including MNIST²⁸, Fashion MNIST²⁹, and CIFAR-10³⁰. The datasets consist of ten classes, each with over 50,000 training samples. To transfer knowledge in a federated distillation setting, we randomly select 10% to 20% of the training data from each class as unlabeled proxy samples. In the experiments, ten clients participate in the distillation process, and we evaluate the model’s performance under two non-IID distribution settings across clients: a strong non-IID setting and a weak non-IID setting, where each client has one unique class and two classes, respectively. Several representative federated distillation methods are compared, including FedMD¹², FedED¹⁷, DS-FL¹⁸, FKD³¹, and PLS²³. Among them, FedMD, FedED, and DS-FL rely on a proxy dataset to transfer knowledge, while FKD and PLS are data-free KD approaches that share class-wise average predictions among users. Besides, we report the performance of independent learning (abbreviated as IndepLearn), where each client trains the model on its local dataset. The comparison includes the results of sharing hard labels (predicted labels) and soft labels (normalized logits). We use classification accuracy as a metric for the evaluation. The architectures of local models are heterogeneous. Specifically, in the chest X-ray image, MNIST, and Fashion MNIST classification tasks, the local models are composed of a few convolutional layers and fully-connected layers. For the CIFAR-10 classification task, ResNet³² is adopted as a backbone network for image processing. More details of the datasets and model architectures are deferred to Supplementary Information.

The average test accuracy of clients on the pneumonia detection task is depicted in Fig. 4. It is observed that the proposed Selective-FD method outperforms all the baseline methods by a substantial margin, and the performance gain is more significant when using hard labels to transfer knowledge. For example, sharing knowledge by hard labels and soft labels resulted in improvements of 19.42% and 4.00%, respectively, over the best-performed baseline. This is because the proposed knowledge selection mechanism can adapt to the heterogeneous characteristics of local data, making it effective in selecting useful

Method	MNIST		FashionMNIST		CIFAR-10	
	Hard label	Soft label	Hard label	Soft label	Hard label	Soft label
IndepLearn	10.00±0.00		10.00±0.00		10.00±0.00	
FedMD	18.89±0.30	<u>88.71±0.28</u>	16.54±0.25	<u>64.63±0.37</u>	10.71±0.38	<u>15.78±1.39</u>
FedED	11.49±0.25	<u>11.92±0.41</u>	12.45±0.44	<u>12.52±0.38</u>	<u>11.83±0.26</u>	<u>12.04±0.30</u>
DS-FL	<u>19.72±0.32</u>	35.25±0.36	<u>17.54±0.11</u>	35.98±0.43	10.87±0.25	12.07±0.32
FKD	10.00±0.00	10.00±0.00	10.00±0.00	10.00±0.00	10.00±0.00	10.00±0.00
PLS	10.00±0.00	10.00±0.00	10.00±0.00	10.00±0.00	10.00±0.00	10.00±0.00
Selective-FD	85.92±0.37	94.68±0.52	73.41±0.98	75.31±0.29	80.22±0.74	80.98±0.39

Table 1. Test accuracy of different methods in the **strong non-IID setting**. Each experiment is repeated five times. The results in bold indicate the best performance, while the results underlined represent the second-best performance. The proposed Selective-FD method achieves a significant improvement compared with other baselines. Particularly, the FKD and PLS methods degrade to independent learning, since each client only has one unique class, rendering the class-wise ensemble predictions redundant and providing no additional information for knowledge distillation.

Method	MNIST		FashionMNIST		CIFAR-10	
	Hard label	Soft label	Hard label	Soft label	Hard label	Soft label
IndepLearn	19.96±0.00		19.82±0.01		19.52±0.02	
FedMD	26.77±0.57	<u>95.16±0.52</u>	41.92±0.30	<u>74.83±0.41</u>	62.14±0.22	<u>84.31±0.53</u>
FedED	<u>59.95±1.11</u>	60.26±1.80	32.62±1.09	37.12±0.85	53.11±0.34	56.13±0.14
DS-FL	25.53±1.43	47.87±0.31	23.08±0.23	39.22±0.26	33.22±0.54	52.51±0.70
FKD	19.97±0.01	19.98±0.00	19.54±0.13	19.71±0.07	19.50±0.02	19.51±0.01
PLS	19.96±0.01	19.97±0.00	19.64±0.09	19.70±0.03	19.51±0.01	19.52±0.01
Selective-FD	86.82±0.26	96.30±0.25	75.57±0.61	77.27±0.31	81.06±0.67	85.38±0.35

Table 2. Test accuracy of different methods in the **weak non-IID setting**. Each experiment is repeated five times. The results in bold indicate the best performance, while the results underlined represent the second-best performance. Our Selective-FD method performs better than the baseline methods, and the accuracy gain is more significant when using hard labels in knowledge distillation than soft labels.

knowledge among clients. In contrast, some baselines perform even worse than the independent learning scheme. This finding highlights the potential negative influence of knowledge sharing among clients, which can mislead the local training. Notably, while hard label sharing provides a stronger privacy guarantee³³, soft label sharing provides additional performance gains. This is because soft labels provide more information about the relationships between classes than hard labels, which helps mitigate the problem of misleading knowledge.

We also evaluate the performance of different federated distillation methods on the benchmark image datasets. To compare their effectiveness in handling heterogeneous data, Table 1 and Table 2 report the test accuracy in the strong non-IID setting and weak non-IID setting, respectively. We find that the proposed Selective-FD method consistently outperforms the baselines. In the strong non-IID setting, the improvement of our method is more significant. Meanwhile, the FKD and PLS methods degrade to independent learning in this challenging setting, as each client only possesses one unique class, rendering the class-wise ensemble predictions uninformative.

Effectiveness of Density-Ratio Estimation

We verify the effectiveness of the density-ratio estimation in detecting incorrect predictions of local models. Specifically, as an ablation study, we replace the density-ratio based selector in Selective-FD with confidence-based methods²⁴ and energy-based models (EBMs)²⁵. The confidence score refers to the maximum probability of the logits in the classification task, which reflects the reliability of the prediction. The EBMs distinguish the in-distribution samples and out-distribution samples by learning an underlying probability distribution over the training samples. The predictions of proxy samples detected as out-distribution samples will be ignored.

Our experiments were conducted on benchmark datasets under the strong non-IID setting, where hard labels are shared among clients for distillation. We use the area under the receiver operating characteristic (AUROC) metric to measure the capability of selectors to detect incorrect predictions. In addition, we evaluated the performance of various selectors by reporting test accuracy. As shown on the left-hand side of Fig. 5, the AUROC score of our method is much higher than the baselines. Particularly, the confidence-based method and energy-based model perform only marginally better than random guess

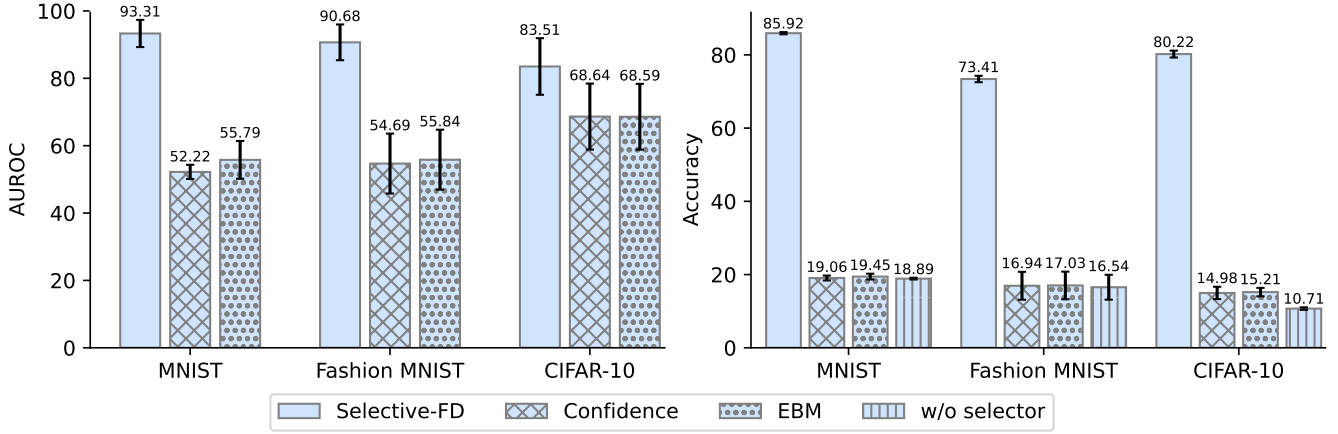


Figure 5. The AUROC scores of different client-side selectors to detect incorrect predictions (left) and the test accuracy after federated distillation (right). The error bar represents the standard deviation across 10 clients. The results show that both the AUROC score and the accuracy of our Selective-FD method are much higher than the baselines, indicating its effectiveness in identifying unknown classes from the proxy dataset and leading to a remarkable performance gain in the federated distillation.

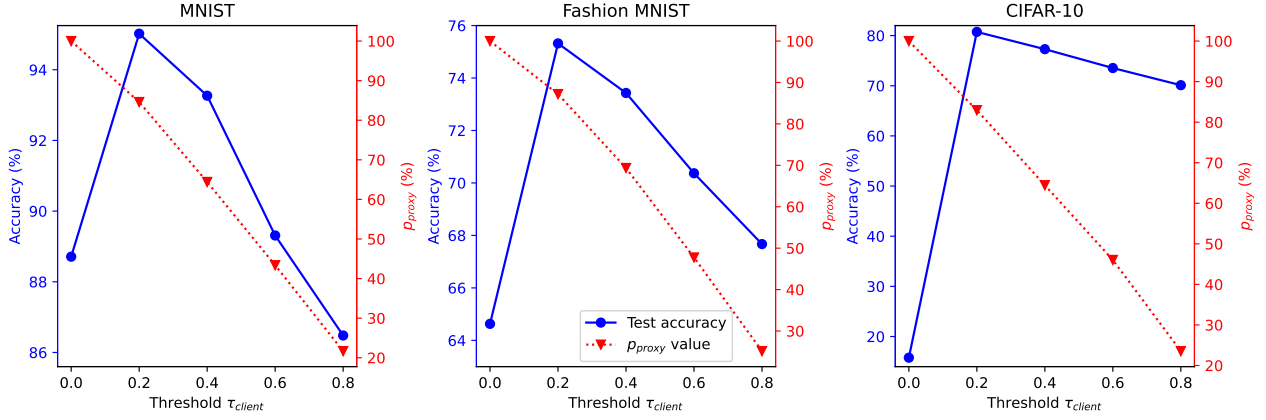
(AUROC= 0.5) on the MNIST and Fashion MNIST datasets. This is because the neural networks tend to be over-confident³⁴ about the predictions, and thus the confidence score may not be able to reflect an accurate probability of correctness for any of its predictions. Besides, the energy-based model fails to detect the incorrect predictions because they often suffer from the problem of overfitting without the out-of-distribution samples³⁵. The right-hand side of Fig. 5 shows the test accuracy after federated distillation. As the density-ratio estimation can effectively identify unknown classes from the proxy samples, the ensemble knowledge is less misleading and our Selective-FD approach achieves a significant performance gain.

Thresholds Analysis

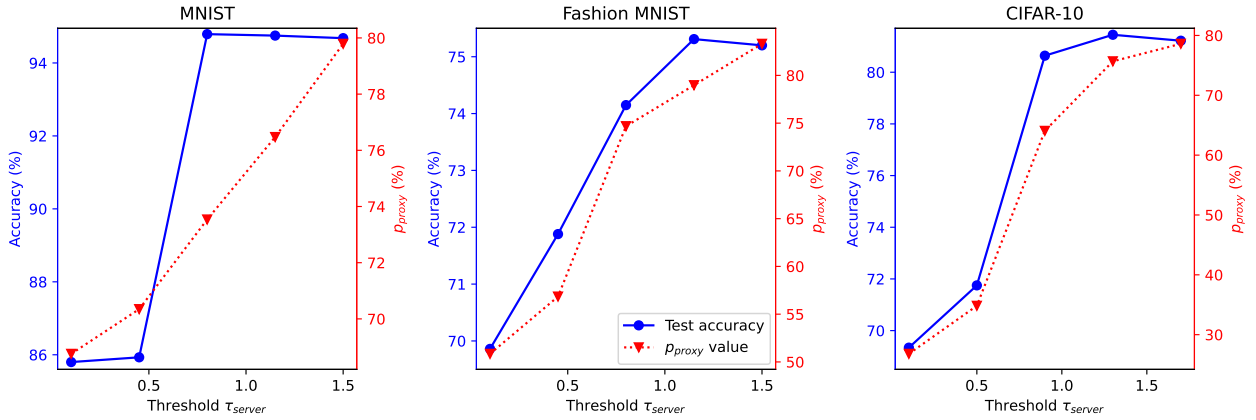
In this study, we investigated the effect of the thresholds τ_{client} and τ_{server} on the performance of the proposed method. Notably, we have reserved a portion of the local data as a validation set to determine the threshold of the client-side selectors. The value of τ_{client} corresponds to the quantile of the estimated ratio over the aforementioned validation set. We conducted experiments on three benchmark image datasets in the strong non-IID setting, where the predictions shared among clients are soft labels. Fig. 6 displays the results, with p_{proxy} representing the percentage of proxy samples used to transfer knowledge after selection. The threshold τ_{client} is set as 0.25 when evaluating the performance of τ_{server} , and the threshold τ_{server} is set as 2 when evaluating the performance of τ_{client} . We have observed that both the values of τ_{client} and τ_{server} have a considerable impact on the performance. When τ_{client} is set too high or τ_{server} is set too low, a significant number of proxy samples are filtered out by the server-side selector, degrading the performance. On the other hand, setting τ_{client} too low may cause the client-side selectors to be unable to remove the inaccurate local predictions, leading to a negative impact on knowledge distillation. Besides, when τ_{server} is set too high, the server-side selector fails to identify the ensemble predictions with high entropy, which results in a drop in accuracy. These empirical results align with Theorem 2 and the analysis presented in Remark 1.

Communication Overhead

We further investigate the communication overhead of the proposed Selective-FD method and compare it with FedAvg⁸, a prevalent FL framework. In each communication round of FedAvg, the clients train their models locally and upload them to the server for aggregation, which requires the local models to share the same architecture. For the MNIST and Fashion MNIST datasets, we initialized the local model as a multilayer perceptron with two hidden layers, each containing 1,024 neurons. For the CIFAR-10 dataset, we used ResNet18 as the local model. Fig. 7 plots the test accuracy and communication overhead with respect to the communication round, where the proxy samples are transmitted in the PNG format, and the local models are compressed in the RAR format. Our Selective-FD method performs comparably to FedAvg in the MNIST and CIFAR-10 datasets, but it is inferior in Fashion MNIST. However, Selective-FD achieves a significant reduction in the communication overhead, which is because the cost of model parameters sharing in FedAvg is much higher than that of proxy samples sharing in the federated distillation methods. The communication cost of FedAvg will further increase if larger models are adopted.



(a) Ablation study on threshold τ_{client} of Selective-FD.



(b) Ablation study on threshold τ_{server} of Selective-FD.

Figure 6. Test accuracy and percentage p_{proxy} under (a) different values of τ_{client} and (b) different values of τ_{server} . We denote the percentage of proxy samples selected for knowledge distillation as p_{proxy} . When τ_{client} is too large or τ_{server} is too small, the selectors filter out most of the proxy samples, leading to a small batch size and increased training variance. Conversely, when τ_{client} is too small, the local outputs may contain an excessive number of incorrect predictions, leading to a decrease in the effectiveness of knowledge distillation. Besides, when τ_{server} is too large, the ensemble predictions may exhibit high entropy, indicating ambiguous knowledge that could degrade local model training. These empirical results align with the analysis in Remark 1.

Discussion

This work introduces the Selective-FD method in federated distillation, which includes a selective knowledge sharing mechanism that identifies accurate and precise knowledge from clients for effective knowledge transfer. The mechanism includes client-side selectors and a server-side selector. The client-side selectors use density-ratio estimators to identify out-of-distribution samples from the proxy dataset. If a sample has a density ratio close to zero, it is considered as an outlier, and the predicted result is not shared to prevent misleading other clients. Although the client-side selectors aim to only share accurate knowledge, the local predictions of proxy samples may be inconsistent among clients, causing the ensemble predictions to have high entropy. In this case, the server-side selector filters out ambiguous predictions and sends the precise ones back to the clients for knowledge distillation. Extensive experiments were conducted on both pneumonia detection and benchmark image classification tasks in non-IID settings to investigate the impact of hard labels and soft labels on the performance of knowledge distillation. The results demonstrate that the proposed Selective-FD method excels in handling non-IID data and significantly improves test accuracy compared to the baselines. The accuracy gain is more prominent in hard label sharing than in soft label sharing. Furthermore, compared with the standard parameter-sharing method in FL, our method reduced the communication cost by up to $900\times$.

While our proposed framework was mainly evaluated on image datasets, it can be applied to general scenarios that involve

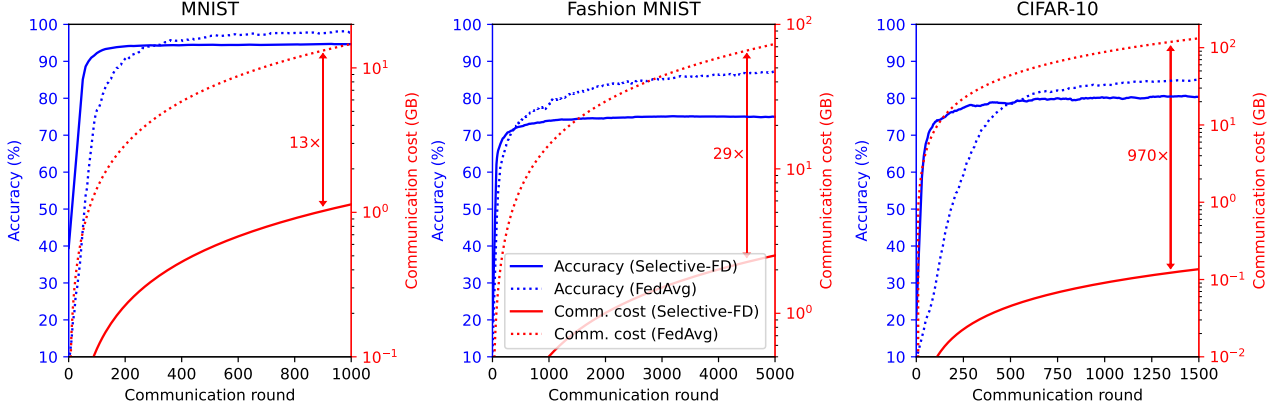


Figure 7. Test accuracy and communication cost as functions of the communication round. Our Selective-FD method has a comparable accuracy as FedAvg in the MNIST and CIFAR-10 datasets but is inferior in Fashion MNIST. However, Selective-FD achieves a significant reduction in the communication overhead, which is because the cost of model sharing in FedAvg is much higher than knowledge sharing in our method.

private user data including personalized recommendations, healthcare, and financial services. Particularly, this method is especially useful for federated training on large models since it does not share model parameters. As deep learning models with more parameters may encode and contain more sensitive information from the private dataset, they are more vulnerable to white-box attacks in FL with model sharing. Moreover, our method is communication-friendly, as it does not require uploading and downloading model parameters. This feature can largely mitigate the communication bottleneck when bandwidth resources are limited. We envision that our proposed method can serve as a template framework for various applications and inspire future research to improve the effectiveness and responsibility of intelligence systems.

There are also several limitations that should be acknowledged. Firstly, the federated distillation method relies on proxy samples to transfer knowledge, which should accurately represent the distributions of local datasets. If the proxy dataset is biased towards certain classes, the client models may be biased toward these classes. This leads to poor performance and generalization. Secondly, the complexity of the client-side selector in our Selective-FD method increases quadratically with the number of samples and the sample space, which limits its practical applicability. Some studies in open-set learning have shown that other low-complexity outlier detection methods, while lacking theoretical guarantees, can achieve comparable performance in outlier detection. This finding motivates us to explore more efficient selectors in future research.

Ethical and societal Impact

It is essential to note that the proposed federated distillation framework, like other AI algorithms, is a dual-use technology. Although the objective is to facilitate the training process of deep learning models by effectively sharing knowledge among clients, this technology can also be misused. Firstly, federated distillation could be used to train algorithms among malicious entities to identify individuals illegally and monitor the speaking patterns of people without their consent³⁶. This poses threats to individual freedom and civil liberties. Secondly, it is assumed that all the participants in federated distillation, including the clients and the server, are trusted and behave honestly. However, if a group of clients or the server are malicious, they could manipulate the local predictions and add poison knowledge during the training process, heavily degrading the model performance of other clients^{37,38}. Thirdly, while federated distillation is free of white-box attacks, it is still potentially vulnerable to black-box attacks such as membership inference attacks³³. This is because the local predictions are shared among clients, which may allow an attacker to infer whether a particular sample was part of a client’s training set or not. To mitigate this vulnerability, additional privacy-preserving techniques such as differential privacy or secure aggregation can be used to further protect the privacy of the local data. Furthermore, there are concerns about the collection of proxy samples to transfer knowledge between clients, particularly if these samples contain sensitive or personal data. This could potentially lead to breaches of privacy and security, as well as ethical concerns regarding informed consent and data ownership. In summary, while the proposed federated distillation framework has great potential for facilitating the training process of deep learning models, it is important to be aware of the potential risks and take measures to mitigate them to ensure that the technology is used ethically and responsibly.

Methods

In this section, we provide an in-depth introduction to our proposed method. We first define the problem studied in this paper, then introduce the details of our method, and provide theoretical insights to discuss the impact of the selective knowledge sharing mechanism on generalization.

Notations and Problem Definition

Consider a federated setting for multi-class classification where each input instance has one ground truth label from C categories. We index clients as $1, 2, \dots, K$, where the k -th client stores a private dataset \mathcal{D}_k , consisting of m_k data points sampled from the distribution \mathcal{D}_k . In addition, there is a proxy dataset $\mathcal{D}_{\text{proxy}}$ containing m_{proxy} samples from the distribution $\mathcal{D}_{\text{proxy}}$ to transfer knowledge among clients. We denote \mathcal{X} as the input space and $\mathcal{Y} \in V(\Delta^{C-1})$ as the label space. Specifically, $V(\Delta^{C-1})$ is a vertex set consisting of all vertices in a $C-1$ simplex Δ^{C-1} , where each vertex corresponds to a one-hot vector. We assume that all the local datasets and the test dataset have the same labeling function $\hat{\mathbf{h}}^* : \mathcal{X} \rightarrow V(\Delta^{C-1})$. Client k learns a local predictor $\mathbf{h}_k : \mathcal{X} \rightarrow \Delta^{C-1}$ to approach $\hat{\mathbf{h}}^*$ in the training phase and outputs a one-hot vector by $\hat{\mathbf{h}}_k : \mathcal{X} \rightarrow V(\Delta^{C-1})$ in the test phase. The hypothesis spaces of \mathbf{h}_k and $\hat{\mathbf{h}}_k$ are \mathcal{H}_k and $\hat{\mathcal{H}}_k$, respectively, which are determined by the parameter spaces of the personalized models. During the process of knowledge sharing, we define the labeling function of the proxy samples as $\mathbf{h}_{\text{proxy}}^* : \mathcal{X} \rightarrow \Delta^{C-1}$, which is determined by both the local predictors and the knowledge selection mechanism. To facilitate the theoretical analysis, we adopt $\hat{\mathbf{h}}_{\text{proxy}}^* : \mathcal{X} \rightarrow V(\Delta^{C-1})$ as the one-hot output of $\mathbf{h}_{\text{proxy}}^*$.

In the experiments, we use cross entropy as the loss function, while for the sake of mathematical traceability, the ℓ_1 norm is adopted to measure the difference between two predictors, denoted by $\mathcal{L}_{\mathcal{D}}(\hat{\mathbf{h}}, \hat{\mathbf{h}}') := \mathbb{E}_{\mathbf{x} \sim \mathcal{D}} \|\hat{\mathbf{h}}(\mathbf{x}) - \hat{\mathbf{h}}'(\mathbf{x})\|_1$, where \mathcal{D} is the distribution. Specifically, $\mathcal{L}_{\mathcal{D}_{\text{test}}}(\hat{\mathbf{h}}_k, \hat{\mathbf{h}}^*)$, $\mathcal{L}_{\mathcal{D}_k}(\hat{\mathbf{h}}_k, \hat{\mathbf{h}}')$, and $\mathcal{L}_{\mathcal{D}_{\text{proxy}}}(\hat{\mathbf{h}}_k, \mathbf{h}_{\text{proxy}}^*)$ represent the loss over the test distribution, local samples, and the proxy samples, respectively. Besides, we define the training loss over both the private and proxy samples as $\mathcal{L}_{\hat{\mathcal{D}}_k \cup \hat{\mathcal{D}}_{\text{proxy}}}(\hat{\mathbf{h}}_k) := \alpha \mathcal{L}_{\hat{\mathcal{D}}_k}(\hat{\mathbf{h}}_k, \hat{\mathbf{h}}^*) + (1 - \alpha) \mathcal{L}_{\hat{\mathcal{D}}_{\text{proxy}}}(\hat{\mathbf{h}}_k, \mathbf{h}_{\text{proxy}}^*)$, where $\alpha \in [0, 1]$ is a weighted coefficient. The notation $\Pr_{\mathcal{D}}[\cdot]$ represents the probability of events over the distribution \mathcal{D} .

Selective Knowledge Sharing in Federated Distillation

Federated distillation aims at collaboratively training models among clients by sharing knowledge, instead of sharing models as in FL. The training process involves two phases. First, the clients train the local models independently on the local data. Then, the clients share knowledge among themselves based on a proxy dataset and fine-tune the local models over both the local and proxy samples. Figure 1 provides an overview of our Selective-FD framework, which includes a selective knowledge sharing mechanism. The following section will delve into the details of this mechanism.

Client-Side Selector

Federated distillation presents a challenge of misleading ensemble predictions caused by the lack of a well-trained teacher. Local models may overfit the local datasets, leading to poor generalization on proxy samples outside the local distribution, especially with non-iid data across clients. To mitigate this issue, our method develops client-side selectors to identify proxy samples that are out of the local distribution (OOD). This is done through density-ratio estimation^{39,40}, which calculates the ratio of two probability densities. Assuming the input data space \mathcal{X} is compact, we define \mathcal{U} as a uniform distribution with probability density function $u(\mathbf{x})$ over \mathcal{X} . Besides, we denote the probability density function at client k as $p_k(\mathbf{x})$. Our objective is to estimate the density ratio $\mathbf{w}_k^*(\mathbf{x}) = p_k(\mathbf{x})/u(\mathbf{x})$ based on the observed samples. Specifically, the in-sample data \mathbf{x} from the local distribution with $p_k(\mathbf{x}) > 0$ results in $\mathbf{w}_k^*(\mathbf{x}) > 0$, while the OOD samples \mathbf{x} with probability $p_k(\mathbf{x}) = 0$ leads to $\mathbf{w}_k^*(\mathbf{x}) = 0$. Therefore, the clients can build density-ratio estimators to identify the OOD samples from the proxy dataset.

Considering the property of statistical convergence, we use a kernelized variant of unconstrained least-squares importance fitting (KuLSIF)²⁶ to estimate the density ratio. The estimation model in KuLSIF is a reproducing kernel Hilbert space (RKHS)⁴¹ \mathcal{W}_k endowed with a Gaussian kernel function. We sample n_k and n_u data points from \mathcal{D}_k and \mathcal{U} , respectively, and denote the resulting sample sets as S_k and S_u . Defining the norm on \mathcal{W}_k as $\|\cdot\|_{\mathcal{W}_k}$, the density-ratio estimator \mathbf{w}_k is obtained as an optimal solution of

$$\mathbf{w}_k = \underset{\mathbf{w}_k \in \mathcal{W}_k}{\operatorname{argmin}} \frac{1}{2n_u} \sum_{\mathbf{x} \sim S_u} (\mathbf{w}_k'(\mathbf{x}))^2 - \frac{1}{n_k} \sum_{\mathbf{x} \sim S_k} \mathbf{w}_k'(\mathbf{x}) + \frac{\beta}{2} \|\mathbf{w}_k'\|_{\mathcal{W}_k}^2, \quad (1)$$

where the analytic-form solution \mathbf{w}_k is available in Theorem 1 of the KuLSIF method²⁶. The following theorem reveals the convergence rate of the KuLSIF estimator.

Theorem 1. (Convergence rate of KuLSIF²⁶). Consider RKHS \mathcal{W}_k to be the Hilbert space with Gaussian kernel that contains the density ratio \mathbf{w}_k^* . Given $\delta \in (0, 1)$ and setting the regularization $\beta = \beta_{n_k, n_u}$ such that $\lim_{n_k, n_u \rightarrow 0} \beta_{n_k, n_u} = 0$ and $\beta_{n_k, n_u}^{-1} = O(\min\{n_k, n_u\}^{1-\delta})$, we have $\mathbb{E}_{\mathbf{x} \sim u(\mathbf{x})} \|\mathbf{w}_k(\mathbf{x}) - \mathbf{w}_k^*(\mathbf{x})\| = O_p(\beta_{n_k, n_u}^{1/2})$, where O_p is the probability order.

The proof is available in Theorem 2 of the KuLSIF method²⁶. This theorem demonstrates that as the number of samples increases and the regularization parameter β_{n_k, n_u} approaches zero, the estimator \mathbf{w}_k converges to the density ratio \mathbf{w}_k^* . During federated distillation, we use a threshold $\tau_{\text{client}} > 0$ to distinguish between in-distribution and out-of-distribution samples. If the estimated $\mathbf{w}_k(\mathbf{x})$ value of a proxy sample \mathbf{x} is below τ_{client} , it is considered as an out-of-distribution sample at client k . In such cases, the client-side selector does not upload the corresponding local prediction as it could be misleading.

Server-Side Selector

After receiving local predictions from clients, the server averages them to produce the ensemble predictions. For each proxy sample \mathbf{x} , the ensemble prediction is denoted as $\mathbf{h}_{\text{proxy}}^*(\mathbf{x}) \in \Delta^{C-1}$, and the corresponding one-hot prediction is represented as $\hat{\mathbf{h}}_{\text{proxy}}^*(\mathbf{x}) \in V(\Delta^{C-1})$. It is important to note that if the local predictions for a specific proxy sample differ greatly among clients, the resulting ensemble prediction $\mathbf{h}_{\text{proxy}}^*(\mathbf{x})$ could be ambiguous with high entropy. This ambiguity could negatively impact knowledge distillation. To address this issue, we developed a server-side selector that measures sample ambiguity by calculating the ℓ_1 distance between $\mathbf{h}_{\text{proxy}}^*(\mathbf{x})$ and $\hat{\mathbf{h}}_{\text{proxy}}^*(\mathbf{x})$. The closer this distance is to zero, the less ambiguous the prediction is. In the proposed Selective-FD framework, the server-side selector applies a threshold $\tau_{\text{server}} > 0$ to filter out ambiguous knowledge, where the ensemble predictions with an ℓ_1 distance greater than τ_{server} will not be sent back to the clients for distillation.

Theoretical Insights

In this section, we establish an upper bound for the loss of federated distillation, while also discussing the effectiveness of the proposed selective knowledge sharing mechanism in the context of domain adaptation⁴². To ensure clarity, we begin by providing relevant definitions before delving into the analysis.

Definition 1. (Minimum combined loss) The ideal predictor in the hypothesis space \mathcal{H}_k achieves the minimum combined loss λ over the test and training sets. Two representative $\lambda_k, \lambda_{k, \text{proxy}}$ are defined as follows:

$$\lambda_k = \min_{\hat{\mathbf{h}}_k \in \mathcal{H}_k} \left\{ \mathcal{L}_{\mathcal{D}_{\text{test}}}(\hat{\mathbf{h}}_k, \mathbf{h}^*) + \mathcal{L}_{\mathcal{D}_k}(\hat{\mathbf{h}}_k, \mathbf{h}^*) \right\}, \quad \lambda_{k, \text{proxy}} = \min_{\hat{\mathbf{h}}_k \in \mathcal{H}_k} \left\{ \mathcal{L}_{\mathcal{D}_{\text{test}}}(\hat{\mathbf{h}}_k, \mathbf{h}^*) + \mathcal{L}_{\mathcal{D}_{\text{proxy}}}(\hat{\mathbf{h}}_k, \mathbf{h}^*) \right\}. \quad (2)$$

The ideal predictor serves as an indicator of the learning ability of the local model. If the ideal predictor performs poorly, it is unlikely that the locally optimized model, which minimizes the training loss, will generalize well on the test set. On the other hand, when the labeling function $\hat{\mathbf{h}}^*$ belongs to the hypothesis space \mathcal{H}_k , we get the minimum loss as $\lambda_k = \lambda_{k, \text{proxy}} = 0$. The next two definitions aim at introducing a metric for measuring the distance between distributions.

Definition 2. (Hypothesis space \mathcal{G}_k) For a hypothesis space \mathcal{H}_k , we define a set of hypotheses $g_k : \mathcal{X} \rightarrow \{0, 1\}$ as \mathcal{G}_k , where $g_k(\mathbf{x}) = \frac{1}{2} \|\hat{\mathbf{h}}_k(\mathbf{x}) - \hat{\mathbf{h}}_k'(\mathbf{x})\|_1$ for $\hat{\mathbf{h}}_k, \hat{\mathbf{h}}_k' \in \mathcal{H}_k$.

Definition 3. (\mathcal{G}_k -distance⁴³) Given two distributions \mathcal{D} and \mathcal{D}' over \mathcal{X} , let $\mathcal{G}_k = \{g_k : \mathcal{X} \rightarrow \{0, 1\}\}$ be a hypothesis space, and the \mathcal{G}_k -distance between \mathcal{D} and \mathcal{D}' is $d_{\mathcal{G}_k}(\mathcal{D}, \mathcal{D}') = 2 \sup_{g_k \in \mathcal{G}_k} |\Pr_{\mathcal{D}}[g_k(\mathbf{x}) = 1] - \Pr_{\mathcal{D}'}[g_k(\mathbf{x}) = 1]|$.

With the above preparations, we derive an upper bound of the test loss of the predictor $\hat{\mathbf{h}}_k$ at client k following the process of federated distillation.

Theorem 2. With probability at least $1 - \delta$, $\delta \in (0, 1)$, we have

$$\mathcal{L}_{\mathcal{D}_{\text{test}}}(\hat{\mathbf{h}}_k, \mathbf{h}^*) \leq \underbrace{\mathcal{L}_{\hat{\mathcal{D}}_k \cup \hat{\mathcal{D}}_{\text{proxy}}}(\hat{\mathbf{h}}_k)}_{\text{Empirical risk}} + \underbrace{\sqrt{\left(\frac{2\alpha^2}{m_k} + \frac{2(1-\alpha)^2}{m_{\text{proxy}}} \right) \log \frac{2}{\delta}}}_{\text{Numerical constraint}} + \alpha [\lambda_k + d_{\mathcal{G}_k}(\mathcal{D}_k, \mathcal{D}_{\text{test}})] \quad (3)$$

$$+ (1 - \alpha) \left[\lambda_{k, \text{proxy}} + d_{\mathcal{G}_k}(\mathcal{D}_{\text{proxy}}, \mathcal{D}_{\text{test}}) + \underbrace{p_{\text{proxy}}^{(1)} \mathcal{L}_{\mathcal{D}_{\text{proxy}}^{(1)}}(\hat{\mathbf{h}}^*, \mathbf{h}_{\text{proxy}}^*)}_{\text{Misleading knowledge}} + \underbrace{p_{\text{proxy}}^{(2)} \mathcal{L}_{\mathcal{D}_{\text{proxy}}^{(2)}}(\hat{\mathbf{h}}_{\text{proxy}}^*, \mathbf{h}_{\text{proxy}}^*)}_{\text{Ambiguous knowledge}} \right], \quad (4)$$

where the probabilities $p_{\text{proxy}}^{(1)} = \Pr_{\mathcal{D}_{\text{proxy}}}[\hat{\mathbf{h}}^*(\mathbf{x}) \neq \hat{\mathbf{h}}_{\text{proxy}}^*(\mathbf{x})]$ and $p_{\text{proxy}}^{(2)} = \Pr_{\mathcal{D}_{\text{proxy}}}[\hat{\mathbf{h}}^*(\mathbf{x}) = \hat{\mathbf{h}}_{\text{proxy}}^*(\mathbf{x})]$ satisfy $p_{\text{proxy}}^{(1)} + p_{\text{proxy}}^{(2)} = 1$. $\mathcal{D}_{\text{proxy}}^{(1)}$ and $\mathcal{D}_{\text{proxy}}^{(2)}$ represent the conditional distributions of proxy samples given $\hat{\mathbf{h}}^*(\mathbf{x}) \neq \hat{\mathbf{h}}_{\text{proxy}}^*(\mathbf{x})$ and $\hat{\mathbf{h}}^*(\mathbf{x}) = \hat{\mathbf{h}}_{\text{proxy}}^*(\mathbf{x})$, respectively.

In (3), the first term on the right-hand side represents the empirical risk over the local and proxy samples, and the second term is a numerical constraint, which indicates that having more proxy samples, whose number is denoted as m_{proxy} , is beneficial to the generalization performance. The last two terms in (4) account for the misleading and ambiguous knowledge

in distillation. From Theorem 2, two key implications can be drawn. Firstly, when there is severe data heterogeneity, the resulting high distribution divergence $d_{\mathcal{G}_k}(\mathcal{D}_k, \mathcal{D}_{\text{test}}), d_{\mathcal{G}_k}(\mathcal{D}_{\text{proxy}}, \mathcal{D}_{\text{test}})$ undermines generalization performance. When the proxy distribution is closer to the test set than the local data, i.e., $d_{\mathcal{G}_k}(\mathcal{D}_k, \mathcal{D}_{\text{test}}) \geq d_{\mathcal{G}_k}(\mathcal{D}_{\text{proxy}}, \mathcal{D}_{\text{test}})$, federated distillation can improve performance compared to independent training. Secondly, if the labeling function (i.e., the ensemble prediction) $\mathbf{h}_{\text{proxy}}^*$ of the proxy samples is highly different from the labeling function $\hat{\mathbf{h}}^*$ of test samples, the error introduced by the misleading and ambiguous knowledge can be significant, leading to negative knowledge transfer. Our proposed selective knowledge sharing mechanism aims to make the ensemble predictions of unlabeled proxy samples closer to the ground truths. Particularly, a large threshold τ_{client} can mitigate the effect of incorrect predictions, while a small threshold τ_{server} implies less ambiguous knowledge being used for distillation.

Remark 1. Care must be taken when setting the thresholds τ_{client} and τ_{server} , as a τ_{client} that is too large or a τ_{server} that is too small could filter out too many proxy samples and result in a small m_{proxy} . This would enlarge the second term on the right-hand side of (3). Additionally, the threshold τ_{server} effectively balances the losses caused by the misleading and ambiguous knowledge, as indicated by the inequalities $2 - \tau_{\text{server}} \leq \|\hat{\mathbf{h}}^*(\mathbf{x}) - \mathbf{h}_{\text{proxy}}^*(\mathbf{x})\|_1$ and $\|\hat{\mathbf{h}}_{\text{proxy}}^*(\mathbf{x}) - \mathbf{h}_{\text{proxy}}^*(\mathbf{x})\|_1 \leq \tau_{\text{server}}$. This property aligns with the empirical results presented in Figure 6.

Remark 2. The proposed mechanism for selectively sharing knowledge and its associated thresholds $\tau_{\text{client}}, \tau_{\text{server}}$ might alter the distributions $\mathcal{D}_{\text{proxy}}, \hat{\mathcal{D}}_{\text{proxy}}$, thus influencing the empirical risk, the minimum combined loss, the \mathcal{G}_k -distance, and the probabilities $p_{\text{proxy}}^{(1)}, p_{\text{proxy}}^{(2)}$ in Theorem 2. A more comprehensive and rigorous analysis of these effects is left to our future work.

References

1. LeCun, Y., Bengio, Y. & Hinton, G. Deep learning. *nature* **521**, 436–444 (2015).
2. Razzak, M. I., Naz, S. & Zaib, A. Deep learning for medical image processing: Overview, challenges and the future. *Classif. BioApps: Autom. Decis. Mak.* 323–350 (2018).
3. Coronato, A., Naeem, M., De Pietro, G. & Paragliola, G. Reinforcement learning for intelligent healthcare applications: A survey. *Artif. Intell. Medicine* **109**, 101964 (2020).
4. Murphy, R. R. *Introduction to AI robotics* (MIT press, 2019).
5. Voigt, P. & Von dem Bussche, A. The EU general data protection regulation (GDPR). *A Pract. Guid. 1st Ed., Cham: Springer Int. Publ.* **10**, 10–5555 (2017).
6. Pardau, S. L. The california consumer privacy act: Towards a European-style privacy regime in the United States. *J. Tech. L. & Pol’y* **23**, 68 (2018).
7. Act, A. Health insurance portability and accountability act of 1996. *Public law* **104**, 191 (1996).
8. McMahan, B., Moore, E., Ramage, D., Hampson, S. & y Arcas, B. A. Communication-efficient learning of deep networks from decentralized data. In *Artificial intelligence and statistics*, 1273–1282 (PMLR, 2017).
9. Li, T. *et al.* Federated optimization in heterogeneous networks. *Proc. Mach. learning systems* **2**, 429–450 (2020).
10. Luping, W., Wei, W. & Bo, L. Cmf1: Mitigating communication overhead for federated learning. In *2019 IEEE 39th international conference on distributed computing systems (ICDCS)*, 954–964 (IEEE, 2019).
11. Liu, L., Zhang, J., Song, S. & Letaief, K. B. Client-edge-cloud hierarchical federated learning. In *ICC 2020-2020 IEEE International Conference on Communications (ICC)*, 1–6 (IEEE, 2020).
12. Li, D. & Wang, J. Fedmd: Heterogenous federated learning via model distillation. *arXiv preprint arXiv:1910.03581* (2019).
13. Dennis, D. K., Li, T. & Smith, V. Heterogeneity for the win: One-shot federated clustering. In *International Conference on Machine Learning*, 2611–2620 (PMLR, 2021).
14. Nasr, M., Shokri, R. & Houmansadr, A. Comprehensive privacy analysis of deep learning: Passive and active white-box inference attacks against centralized and federated learning. In *2019 IEEE symposium on security and privacy (SP)*, 739–753 (IEEE, 2019).
15. Huang, Y., Gupta, S., Song, Z., Li, K. & Arora, S. Evaluating gradient inversion attacks and defenses in federated learning. *Adv. Neural Inf. Process. Syst.* **34**, 7232–7241 (2021).
16. Gou, J., Yu, B., Maybank, S. J. & Tao, D. Knowledge distillation: A survey. *Int. J. Comput. Vis.* **129**, 1789–1819 (2021).

17. Sui, D. *et al.* Feded: Federated learning via ensemble distillation for medical relation extraction. In *Proceedings of the 2020 conference on empirical methods in natural language processing (EMNLP)*, 2118–2128 (2020).
18. Itahara, S., Nishio, T., Koda, Y., Morikura, M. & Yamamoto, K. Distillation-based semi-supervised federated learning for communication-efficient collaborative training with non-iid private data. *IEEE Transactions on Mob. Comput.* **22**, 191–205 (2021).
19. Liu, L., Zhang, J., Song, S. & Letaief, K. B. Communication-efficient federated distillation with active data sampling. In *ICC 2022-IEEE International Conference on Communications*, 201–206 (IEEE, 2022).
20. Papernot, N., Abadi, M., Erlingsson, Ú., Goodfellow, I. & Talwar, K. Semi-supervised knowledge transfer for deep learning from private training data. In *International Conference on Learning Representations*.
21. Zhu, H., Xu, J., Liu, S. & Jin, Y. Federated learning on non-iid data: A survey. *Neurocomputing* **465**, 371–390 (2021).
22. Shao, J., Sun, Y., Li, S. & Zhang, J. Dres-fl: Dropout-resilient secure federated learning for non-iid clients via secret data sharing. In *Advances in Neural Information Processing Systems*.
23. Wang, D., Zhang, N., Tao, M. & Chen, X. Knowledge selection and local updating optimization for federated knowledge distillation with heterogeneous models. *IEEE J. Sel. Top. Signal Process.* **17**, 82–97 (2023).
24. DeVries, T. & Taylor, G. W. Learning confidence for out-of-distribution detection in neural networks. *arXiv preprint arXiv:1802.04865* (2018).
25. Liu, W., Wang, X., Owens, J. & Li, Y. Energy-based out-of-distribution detection. *Adv. neural information processing systems* **33**, 21464–21475 (2020).
26. Kanamori, T., Suzuki, T. & Sugiyama, M. Statistical analysis of kernel-based least-squares density-ratio estimation. *Mach. Learn.* **86**, 335–367 (2012).
27. Wang, L., Lin, Z. Q. & Wong, A. Covid-net: a tailored deep convolutional neural network design for detection of covid-19 cases from chest x-ray images. *Sci. Reports* **10**, 19549, [10.1038/s41598-020-76550-z](https://doi.org/10.1038/s41598-020-76550-z) (2020).
28. LeCun, Y., Bottou, L., Bengio, Y. & Haffner, P. Gradient-based learning applied to document recognition. *Proc. IEEE* **86**, 2278–2324 (1998).
29. Xiao, H., Rasul, K. & Vollgraf, R. Fashion-mnist: a novel image dataset for benchmarking machine learning algorithms. *arXiv preprint arXiv:1708.07747* (2017).
30. Krizhevsky, A., Hinton, G. *et al.* Learning multiple layers of features from tiny images. Preprint at <https://www.cs.toronto.edu/~kriz/learning-features-2009-TR.pdf> (2009).
31. Seo, H., Park, J., Oh, S., Bennis, M. & Kim, S.-L. Federated knowledge distillation. *Mach. Learn. Wirel. Commun.* 457 (2022).
32. He, K., Zhang, X., Ren, S. & Sun, J. Deep residual learning for image recognition. In *Proceedings of the IEEE conference on computer vision and pattern recognition*, 770–778 (2016).
33. Choquette-Choo, C. A., Tramer, F., Carlini, N. & Papernot, N. Label-only membership inference attacks. In *International conference on machine learning*, 1964–1974 (PMLR, 2021).
34. Guo, C., Pleiss, G., Sun, Y. & Weinberger, K. Q. On calibration of modern neural networks. In *International conference on machine learning*, 1321–1330 (PMLR, 2017).
35. Arbel, M., Zhou, L. & Gretton, A. Generalized energy based models. In *International Conference on Learning Representations*.
36. King, T. C., Aggarwal, N., Taddeo, M. & Floridi, L. Artificial intelligence crime: An interdisciplinary analysis of foreseeable threats and solutions. *Sci. engineering ethics* **26**, 89–120 (2020).
37. Tolpegin, V., Truex, S., Gursoy, M. E. & Liu, L. Data poisoning attacks against federated learning systems. In *Computer Security—ESORICS 2020: 25th European Symposium on Research in Computer Security, ESORICS 2020, Guildford, UK, September 14–18, 2020, Proceedings, Part I* 25, 480–501 (Springer, 2020).
38. Fang, M., Cao, X., Jia, J. & Gong, N. Z. Local model poisoning attacks to byzantine-robust federated learning. In *Proceedings of the 29th USENIX Conference on Security Symposium*, 1623–1640 (2020).
39. Sugiyama, M., Suzuki, T. & Kanamori, T. *Density ratio estimation in machine learning* (Cambridge University Press, 2012).

- 40. Fang, Z., Lu, J., Liu, A., Liu, F. & Zhang, G. Learning bounds for open-set learning. In *International conference on machine learning*, 3122–3132 (PMLR, 2021).
- 41. Berline, A. & Thomas-Agnan, C. *Reproducing kernel Hilbert spaces in probability and statistics* (Springer Science & Business Media, 2011).
- 42. Ben-David, S. *et al.* A theory of learning from different domains. *Mach. learning* **79**, 151–175 (2010).
- 43. Kifer, D., Ben-David, S. & Gehrke, J. Detecting change in data streams. In *VLDB*, vol. 4, 180–191 (Toronto, Canada, 2004).

Code Availability

The code used for this work is available from the first author upon reasonable request. We plan to release the code to the public after the manuscript has been published. All experiments and implementation details are thoroughly described in the Experiments section, Methods section, and Supplementary Information.

Data Availability

The datasets used in this paper are publicly available. The COVIDx data is available at <https://www.kaggle.com/datasets/andyczhao/covidx-cxr2>. The benchmark datasets MNIST, Fashion MNIST, and CIFAR-10 are available at <http://yann.lecun.com/exdb/mnist/>, <https://github.com/zalandoresearch/fashion-mnist>, and <https://www.cs.toronto.edu/~kriz/cifar.html>, respectively. The usage of these datasets in this work is permitted under their licenses.

Author contributions statement

J.Z. coordinated and supervised the research project. J.S. conceived the idea of this work, implemented the models for experiments, and analyzed the results. All the authors contributed to the writing of this manuscript.

Additional information

Supplementary Information: The attached files contain the supplementary material.

Competing interests: The authors declare no competing interests.

Supplementary Material

Proof of Theorem 2

Prior to proving Theorem 2, we first present two Lemmas.

Lemma 1. Given hypothesis spaces $\mathcal{H} := \{\hat{\mathbf{h}}: \mathcal{X} \rightarrow V(\Delta^{C-1})\}$ and $\mathcal{G} := \{g: \mathcal{X} \rightarrow \{0, 1\}\}$ with $g(\mathbf{x}) = \frac{1}{2} \|\hat{\mathbf{h}}(\mathbf{x}) - \hat{\mathbf{h}}'(\mathbf{x})\|_1$ for $\hat{\mathbf{h}}, \hat{\mathbf{h}}' \in \mathcal{H}$, we have $|\mathcal{L}_{\mathcal{D}}(\hat{\mathbf{h}}, \hat{\mathbf{h}}') - \mathcal{L}_{\mathcal{D}'}(\hat{\mathbf{h}}, \hat{\mathbf{h}}')| \leq d_{\mathcal{G}}(\mathcal{D}, \mathcal{D}')$ for $\hat{\mathbf{h}}, \hat{\mathbf{h}}' \in \mathcal{H}$.

Proof.

$$\begin{aligned} d_{\mathcal{G}}(\mathcal{D}, \mathcal{D}') &= 2 \sup_{g \in \mathcal{G}} |\Pr_{\mathcal{D}}[g(\mathbf{x}) = 1] - \Pr_{\mathcal{D}'}[g(\mathbf{x}) = 1]|, \\ &= \sup_{\hat{\mathbf{h}}, \hat{\mathbf{h}}' \in \mathcal{H}} 2 \left| \frac{1}{2} \mathbb{E}_{\mathbf{x} \sim \mathcal{D}} [\hat{\mathbf{h}}(\mathbf{x}) - \hat{\mathbf{h}}'(\mathbf{x})] - \frac{1}{2} \mathbb{E}_{\mathbf{x} \sim \mathcal{D}'} [\hat{\mathbf{h}}(\mathbf{x}) - \hat{\mathbf{h}}'(\mathbf{x})] \right| \geq |\mathcal{L}_{\mathcal{D}}(\hat{\mathbf{h}}, \hat{\mathbf{h}}') - \mathcal{L}_{\mathcal{D}'}(\hat{\mathbf{h}}, \hat{\mathbf{h}}')|. \end{aligned}$$

□

Lemma 2. For any $\delta \in (0, 1)$, with probability at least $1 - \delta$ over the choice of the samples, we have

$$\mathcal{L}_{\mathcal{D}_{\text{test}}}(\hat{\mathbf{h}}, \hat{\mathbf{h}}^*) \leq \mathcal{L}_{\hat{\mathcal{D}}_k \cup \hat{\mathcal{D}}_{\text{proxy}}}(\hat{\mathbf{h}}) + \sqrt{\left(\frac{2\alpha^2}{m_k} + \frac{2(1-\alpha)^2}{m_{\text{proxy}}} \right) \log \frac{2}{\delta}}. \quad (5)$$

Proof. The loss $\mathcal{L}_{\hat{\mathcal{D}}_k \cup \hat{\mathcal{D}}_{\text{proxy}}}(\hat{\mathbf{h}})$ can be written as

$$\begin{aligned} \mathcal{L}_{\hat{\mathcal{D}}_k \cup \hat{\mathcal{D}}_{\text{proxy}}}(\hat{\mathbf{h}}) &= \alpha \mathcal{L}_{\hat{\mathcal{D}}_k}(\hat{\mathbf{h}}) + (1 - \alpha) \mathcal{L}_{\hat{\mathcal{D}}_{\text{proxy}}}(\hat{\mathbf{h}}), \\ &= \frac{1}{m_k + m_{\text{proxy}}} \left[\sum_{\mathbf{x} \in \hat{\mathcal{D}}_k} \frac{\alpha(m_k + m_{\text{proxy}})}{m_k} \|\hat{\mathbf{h}}(\mathbf{x}) - \hat{\mathbf{h}}^*(\mathbf{x})\|_1 + \sum_{\mathbf{x} \in \hat{\mathcal{D}}_{\text{proxy}}} \frac{(1 - \alpha)(m_k + m_{\text{proxy}})}{m_{\text{proxy}}} \|\hat{\mathbf{h}}(\mathbf{x}) - \hat{\mathbf{h}}^*(\mathbf{x})\|_1 \right]. \end{aligned} \quad (6)$$

Let $X_1^{(k)}, \dots, X_{m_k}^{(k)}$ and $X_1^{(\text{proxy})}, \dots, X_{m_{\text{proxy}}}^{(\text{proxy})}$ be independent random variables that take on the values of $\frac{\alpha(m_k + m_{\text{proxy}})}{m_k} \|\hat{\mathbf{h}}(\mathbf{x}) - \hat{\mathbf{h}}^*(\mathbf{x})\|_1$ for $\mathbf{x} \in \hat{\mathcal{D}}_k$ and $\frac{(1 - \alpha)(m_k + m_{\text{proxy}})}{m_{\text{proxy}}} \|\hat{\mathbf{h}}(\mathbf{x}) - \hat{\mathbf{h}}^*(\mathbf{x})\|_1$ for $\mathbf{x} \in \hat{\mathcal{D}}_{\text{proxy}}$, respectively. We define \bar{X} as the mean value of these variables, which represents the empirical loss in (6). By linearity of expectations, $\mathbb{E}[\bar{X}]$ is equal to the loss $\mathcal{L}_{\hat{\mathcal{D}}_k \cup \hat{\mathcal{D}}_{\text{proxy}}}(\hat{\mathbf{h}})$. According to Hoeffding's inequality, for any $\varepsilon > 0$, we have

$$\Pr \left[|\mathcal{L}_{\hat{\mathcal{D}}_k \cup \hat{\mathcal{D}}_{\text{proxy}}}(\hat{\mathbf{h}}) - \mathcal{L}_{\hat{\mathcal{D}}_k \cup \hat{\mathcal{D}}_{\text{proxy}}}(\hat{\mathbf{h}})| \geq \varepsilon \right] \leq 2 \exp \left(\frac{-\varepsilon^2}{\frac{2\alpha^2}{m_k} + \frac{2(1-\alpha)^2}{m_{\text{proxy}}}} \right). \quad (7)$$

Let the right-hand side of (7) be δ , we can derive the inequality in Theorem 2. □

We are now ready to prove Theorem 2.

Proof. The following derives the upper bound of $|\mathcal{L}_{\mathcal{D}_{\text{test}}}(\hat{\mathbf{h}}, \hat{\mathbf{h}}^*) - \mathcal{L}_{\mathcal{D}_k \cup \mathcal{D}_{\text{proxy}}}(\hat{\mathbf{h}})|$:

$$\begin{aligned} &|\mathcal{L}_{\mathcal{D}_{\text{test}}}(\hat{\mathbf{h}}, \hat{\mathbf{h}}^*) - \mathcal{L}_{\mathcal{D}_k \cup \mathcal{D}_{\text{proxy}}}(\hat{\mathbf{h}})| = |\mathcal{L}_{\mathcal{D}_{\text{test}}}(\hat{\mathbf{h}}, \hat{\mathbf{h}}^*) - \alpha \mathcal{L}_{\mathcal{D}_k}(\hat{\mathbf{h}}, \hat{\mathbf{h}}^*) - (1 - \alpha) \mathcal{L}_{\mathcal{D}_{\text{proxy}}}(\hat{\mathbf{h}}, \mathbf{h}_{\text{proxy}}^*)|, \\ &\leq \alpha |\mathcal{L}_{\mathcal{D}_{\text{test}}}(\hat{\mathbf{h}}, \hat{\mathbf{h}}^*) - \mathcal{L}_{\mathcal{D}_k}(\hat{\mathbf{h}}, \hat{\mathbf{h}}^*)| + (1 - \alpha) |\mathcal{L}_{\mathcal{D}_{\text{test}}}(\hat{\mathbf{h}}, \hat{\mathbf{h}}^*) - \mathcal{L}_{\mathcal{D}_{\text{proxy}}}(\hat{\mathbf{h}}, \mathbf{h}_{\text{proxy}}^*)|, \\ &\leq \alpha \left[|\mathcal{L}_{\mathcal{D}_k}(\hat{\mathbf{h}}, \hat{\mathbf{h}}^*) - \mathcal{L}_{\mathcal{D}_k}(\hat{\mathbf{h}}, \hat{\mathbf{h}}')| + |\mathcal{L}_{\mathcal{D}_k}(\hat{\mathbf{h}}, \hat{\mathbf{h}}') - \mathcal{L}_{\mathcal{D}_{\text{test}}}(\hat{\mathbf{h}}, \hat{\mathbf{h}}')| + |\mathcal{L}_{\mathcal{D}_{\text{test}}}(\hat{\mathbf{h}}, \hat{\mathbf{h}}') - \mathcal{L}_{\mathcal{D}_{\text{test}}}(\hat{\mathbf{h}}, \hat{\mathbf{h}}^*)| \right], \\ &\quad + (1 - \alpha) \left[|\mathcal{L}_{\mathcal{D}_{\text{proxy}}}(\hat{\mathbf{h}}, \mathbf{h}_{\text{proxy}}^*) - \mathcal{L}_{\mathcal{D}_{\text{proxy}}}(\hat{\mathbf{h}}, \hat{\mathbf{h}}')| + |\mathcal{L}_{\mathcal{D}_{\text{proxy}}}(\hat{\mathbf{h}}, \hat{\mathbf{h}}') - \mathcal{L}_{\mathcal{D}_{\text{test}}}(\hat{\mathbf{h}}, \hat{\mathbf{h}}')| + |\mathcal{L}_{\mathcal{D}_{\text{test}}}(\hat{\mathbf{h}}, \hat{\mathbf{h}}') - \mathcal{L}_{\mathcal{D}_{\text{test}}}(\hat{\mathbf{h}}, \hat{\mathbf{h}}^*)| \right], \\ &\leq \alpha \left[\mathcal{L}_{\mathcal{D}_k}(\hat{\mathbf{h}}, \hat{\mathbf{h}}') + |\mathcal{L}_{\mathcal{D}_k}(\hat{\mathbf{h}}, \hat{\mathbf{h}}') - \mathcal{L}_{\mathcal{D}_{\text{test}}}(\hat{\mathbf{h}}, \hat{\mathbf{h}}')| + \mathcal{L}_{\mathcal{D}_{\text{test}}}(\hat{\mathbf{h}}, \hat{\mathbf{h}}^*) \right], \end{aligned} \quad (8)$$

$$+ (1 - \alpha) \left[\mathcal{L}_{\mathcal{D}_{\text{proxy}}}(\hat{\mathbf{h}}, \mathbf{h}_{\text{proxy}}^*) + |\mathcal{L}_{\mathcal{D}_{\text{proxy}}}(\hat{\mathbf{h}}, \hat{\mathbf{h}}') - \mathcal{L}_{\mathcal{D}_{\text{test}}}(\hat{\mathbf{h}}, \hat{\mathbf{h}}')| + \mathcal{L}_{\mathcal{D}_{\text{test}}}(\hat{\mathbf{h}}, \hat{\mathbf{h}}^*) \right], \quad (9)$$

$$\leq \alpha [\lambda_k + d_{\mathcal{G}_k}(\mathcal{D}_k, \mathcal{D}_{\text{test}})] + (1 - \alpha) \left[\lambda_{k, \text{proxy}} + d_{\mathcal{G}_k}(\mathcal{D}_{\text{proxy}}, \mathcal{D}_{\text{test}}) + \mathcal{L}_{\mathcal{D}_{\text{proxy}}}(\hat{\mathbf{h}}, \mathbf{h}_{\text{proxy}}^*) - \mathcal{L}_{\mathcal{D}_{\text{proxy}}}(\hat{\mathbf{h}}, \hat{\mathbf{h}}^*) \right], \quad (10)$$

$$\leq \alpha [\lambda_k + d_{\mathcal{G}_k}(\mathcal{D}_k, \mathcal{D}_{\text{test}})] + (1 - \alpha) \left[\lambda_{k, \text{proxy}} + d_{\mathcal{G}_k}(\mathcal{D}_{\text{proxy}}, \mathcal{D}_{\text{test}}) + \mathcal{L}_{\mathcal{D}_{\text{proxy}}}(\mathbf{h}_{\text{proxy}}^*, \hat{\mathbf{h}}^*) \right], \quad (11)$$

where

$$\mathcal{L}_{\mathcal{D}_{\text{proxy}}}(\mathbf{h}_{\text{proxy}}^*, \hat{\mathbf{h}}^*) = p_{\text{proxy}}^{(1)} \mathcal{L}_{\mathcal{D}_{\text{proxy}}^{(1)}}(\hat{\mathbf{h}}^*, \mathbf{h}_{\text{proxy}}^*) + p_{\text{proxy}}^{(2)} \mathcal{L}_{\mathcal{D}_{\text{proxy}}^{(2)}}(\hat{\mathbf{h}}_{\text{proxy}}^*, \mathbf{h}_{\text{proxy}}^*). \quad (12)$$

The triangle inequality gives rise to (8), (9), and (11), while Lemma 1 underlies the inequality (10). By combining (11), (12), and Lemma 2, we obtain the upper bound stated in Theorem 2. \square

More Details of Experiments

In the experiments, we use stochastic gradient descent (SGD) with a learning rate of 0.1 as the optimizer. During federated distillation, instead of directly minimizing the empirical loss $\mathcal{L}_{\hat{\mathcal{D}}_k \cup \hat{\mathcal{D}}_{\text{proxy}}}(\hat{\mathbf{h}})$ in Theorem 2, clients begin by training their local models independently based on their datasets for 200 SGD steps. In each communication round, clients then fine-tune the models on local samples and proxy samples for 1 and 10 SGD steps, respectively. This training scheme makes the knowledge distillation process more stable. Table 3 provides a summary of datasets, and the architectures of local models are shown in Table 4, Table 5, and Table 6. The convolutional layer with output channel o , kernel size k , and padding p is denoted as $\text{Conv}(o, k, p)$. The fully-connected layer with output dimension o is defined as $\text{linear}(o)$, and the max-pooling layer with kernel size k is denoted as $\text{MaxPool}(k)$. ReLU represents the rectified linear unit function.

In addition, our method has adopted a portion of the local data as a validation set to determine the threshold τ_{client} of the client-side selectors. The value of τ_{client} corresponds to the quantile of the estimated ratio over the aforementioned validation set. In the weak non-IID scenario, clients are given local training sets containing two classes. As modeling the joint distribution of these classes is challenging and results in high sampling complexity, we utilize an alternative approach where we construct two density-ratio estimators, denoted as $\mathbf{w}_k^{(1)}$ and $\mathbf{w}_k^{(2)}$, for each class. To determine whether a proxy sample should be treated as an in-distribution sample, we apply the same method for selecting the thresholds $\tau_k^{(1)}$ and $\tau_k^{(2)}$ for $\mathbf{w}_k^{(1)}$ and $\mathbf{w}_k^{(2)}$, respectively. If any of the estimators output a density ratio higher than its corresponding threshold, the local prediction of the proxy sample will not be filtered out.

Supplementary Tables

Table 3. Summary of datasets.

	COVIDx	MNIST	Fashion MNIST	CIFAR-10
Number of local data	1000 ~ 2000	5,400	5,400	4,000
Local training batch size	64	64	64	64
Number of proxy data	1,500	6,000	6,000	10,000
Distillation batch size	128	512	512	32

Table 4. The architectures of local models on the pneumonia detection task.

Client 1	Client 2	Client 3	Client 4
Conv(10, 5, 0) + ReLU MaxPool(2)	Conv (10, 3, 1) + ReLU MaxPool(2)	Linear(1024) + ReLU Linear(512) + ReLU	Linear(1024) + ReLU Linear(1024) + ReLU
Conv(20, 5, 0) + ReLU MaxPool(2)	Conv (20, 3, 1) + ReLU MaxPool(2)	Linear(256) + ReLU Linear(3)	Linear(3)
Linear(50) + ReLU Linear(3)	Linear(128) + ReLU Linear(3)		

Table 5. The architectures of local models on the MNIST and Fashion MNIST datasets. Note that the MNIST and Fashion MNIST datasets have images of different sizes, which consequently leads to variations in the input dimensions for the fully-connected layers.

Client 1	Client 2	Client 3	Client 4	Client 5	Client 6	Client 7	Client 8	Client 9	Client 10
Conv(10, 5, 0) ReLU MaxPool(2)	Conv(10, 5, 0) ReLU MaxPool(2)	Conv(10, 3, 1) ReLU MaxPool(2)	Conv(10, 3, 1) ReLU MaxPool(2)	Conv(10, 5, 0) ReLU MaxPool(2)	Conv(10, 5, 0) ReLU MaxPool(2)	Linear(1024) ReLU Linear(512)	Linear(1024) ReLU Linear(512)	Linear(1024) ReLU Linear(1024)	Linear(1024) ReLU Linear(1024)
Conv(20, 5, 0) ReLU MaxPool(2)	Conv(20, 5, 0) ReLU MaxPool(2)	Conv(20, 3, 1) ReLU MaxPool(2)	Conv(20, 3, 1) ReLU MaxPool(2)	Conv(20, 3, 1) ReLU MaxPool(2)	Conv(20, 3, 1) ReLU MaxPool(2)	ReLU Linear(256) ReLU	ReLU Linear(256) ReLU	ReLU Linear(10)	ReLU Linear(10)
Linear(50) ReLU Linear(10)	Linear(50) ReLU Linear(10)	Linear(128) ReLU Linear(10)	Linear(128) ReLU Linear(10)	Linear(64) ReLU Linear(10)	Linear(64) ReLU Linear(10)	Linear(10)	Linear(10)		

Table 6. The architectures of local models on the CIFAR-10 dataset. ResNet* represents the layers of ResNet before the fully connected layer.

Client 1	Client 2	Client 3	Client 4	Client 5	Client 6	Client 7	Client 8	Client 9	Client 10
ResNet*-18 Linear(128) ReLU Linear(64) ReLU Linear(10)	ResNet*-18 Linear(128) ReLU Linear(64) ReLU Linear(10)	ResNet*-18 Linear(256) ReLU Linear(10)	ResNet*-18 Linear(256) ReLU Linear(10)	ResNet*-34 Linear(128) ReLU Linear(64) ReLU Linear(10)	ResNet*-34 Linear(128) ReLU Linear(64) ReLU Linear(10)	ResNet*-34 Linear(256) ReLU Linear(10)	ResNet*-34 Linear(256) ReLU Linear(10)	ResNet*-50 Linear(256) ReLU Linear(10)	ResNet*-50 Linear(256) ReLU Linear(10)